0026-895X/11/8003-476–485$25.00
MOLECULAR PHARMACOLOGY
Copyright © 2011 The American Society for Pharmacology and Experimental Therapeutics
Mol Pharmacol 80:476–485, 2011

Vol. 80, No. 3
72322/3706157
Printed in U.S.A.

Miltefosine Induces Apoptosis-Like Cell Death in Yeast via Cox9p in Cytochrome *c* Oxidase[S]

Xiaoming Zuo, Julianne T. Djordjevic, Johanes Bijosono Oei, Desmarini Desmarini, Stephen D. Schibeci, Katrina A. Jolliffe, and Tania C. Sorrell

Centre for Infectious Diseases and Microbiology (X.Z., J.T.D., J.B.O., D.D., T.C.S.) and Institute for Immunology and Allergy Research (S.D.S.), Westmead Millennium Institute and Sydney Emerging Infections and Biosecurity Institute; and School of Chemistry (K.A.J.), University of Sydney, Sydney, New South Wales, Australia

Received March 17, 2011; accepted May 24, 2011

ABSTRACT

Miltefosine has antifungal properties and potential for development as a therapeutic for invasive fungal infections. However, its mode of action in fungi is poorly understood. We demonstrate that miltefosine is rapidly incorporated into yeast, where it penetrates the mitochondrial inner membrane, disrupting mitochondrial membrane potential and leading to an apoptosis-like cell death. *COX9*, which encodes subunit VIIa of the cytochrome *c* oxidase (COX) complex in the electron transport chain of the mitochondrial membrane, was identified as a potential target of miltefosine from a genomic library screen of the model yeast *Saccharomyces cerevisiae*. When overexpressed in *S. cerevisiae*, *COX9*, but not *COX7* or *COX8*, led to a miltefosine-resistant phenotype. The effect of miltefosine on COX activity was assessed in cells expressing different levels of *COX9*. Miltefosine inhibited COX activity in a dose-dependent manner in Cox9p-positive cells. This inhibition most likely contributed to the miltefosine-induced apoptosis-like cell death.

Introduction

Invasive fungal infections are associated with high morbidity and mortality and are an increasing global health problem. Current therapies are limited in efficacy, antifungal spectrum, and/or safety, and resistant fungi are emerging. Hence, there is an urgent need for new agents. Several novel potential antifungal targets have been identified in recent years, yet only one new class of drug, the echinocandins, has been marketed (Chen and Sorrell, 2007).

Our group has demonstrated that miltefosine (2-[hexadecoxy-oxido-phosphinoyl] oxyethyl-trimethyl-ammonium), which is an alkyl phospholipid and metabolically stable analog of the major eukaryotic cell membrane phospholipid phosphatidylcholine (PC) (van Blitterswijk and Verheij, 2008), has broad-spectrum antifungal activity. Miltefosine was first investigated as an anticancer agent (Unger and Eibl, 1991) and later developed and marketed as an oral treatment for the parasitic disease leishmaniasis (Croft et al., 2003; de Castroa et al., 2004).

Against fungi, minimum inhibitory concentrations (MICs) and minimum fungicidal concentrations of miltefosine were comparable with those of the commonly used drug amphotericin B (Widmer et al., 2006b). Miltefosine was also broadly active against dermatophytes (Tong et al., 2007). The MICs against most pathogenic fungi were well below serum levels achieved by oral miltefosine dosing (Obando et al., 2007). In a single case report, the addition of miltefosine to other antifungal agents as salvage therapy proved effective for treatment of *Scedosporium prolificans* osteomyelitis (Kesson et al., 2009). Although miltefosine shows promise as an antifungal drug, its mode of action, yet to be elucidated, is the key to rational design of more potent and less toxic analogs.

Most of what is known about the mechanism of action of miltefosine comes from studies performed in neoplastic cells (van Blitterswijk and Verheij, 2008) and *Leishmania* spp.

This work was supported by the National Health and Medical Research Council, Australia [Project Grant 570891] and by a Fellowship from the Sydney Medical School Foundation (to T.C.S.).

Article, publication date, and citation information can be found at http://molpharm.aspetjournals.org.

doi:10.1124/mol.111.072322.

[S] The online version of this article (available at http://molpharm.aspetjournals.org) contains supplemental material.

ABBREVIATIONS: PC, phosphatidylcholine; PE, phosphatidylethanolamine; COX, cytochrome *c* oxidase; MIC, minimum inhibitory concentration; YPD, yeast extract peptone dextrose; YPGly, yeast extract peptone glycerol; YNB, yeast nitrogen base; PBS, phosphate-buffered saline; $DiOC_6$, 3,3′-dihexyloxacarbocyanine iodide; DAPI, 4,6-diamidino-2-phenylindole; PI, propidium iodide; TUNEL, terminal deoxynucleotidyl transferase dUTP nick-end labeling; kb, kilobase(s); PCR, polymerase chain reaction; qRT, quantitative real-time; TES, *N*-tris-[hydroxymethyl] methyl-2-aminoethanesulfonic acid; AEBSF, 4-[2-aminoethyl]-benzene-sulfonylfluoride·HCl; KCN, potassium cyanide; WT, wild type; FP, forward primer; RP, reverse primer.

(Barratt et al., 2009). These have revealed a number of poorly defined mechanisms that are different in mammalian and parasitic cells. In neoplastic cell lines, miltefosine is internalized mainly via receptor-independent, membrane-recycling endocytosis, whereas in *Leishmania* spp., it is primarily via a specific membrane transporter, LdMT-LdRos3, a two subunit aminophospholipid translocase with P-type ATPase activity (Pérez-Victoria et al., 2003).

In neoplastic cell lines, because of its phospholipid-like structure, miltefosine is believed to exert its antiproliferative effect by interfering with lipid rafts and proteins in cell membranes. Miltefosine has been reported to inhibit enzymes involved in phospholipid metabolism, including protein kinase C; phospholipases A_2, C, and D; and choline-phosphate cytidylyltransferase in the PC biosynthesis pathway. Miltefosine also triggers signaling pathways that lead to apoptosis (Ruiter et al., 1999) and, at high concentrations, forms pore-like structures on cell membranes, resulting in release of intracellular contents and impairment of cellular homeostasis (Wieder et al., 1999). In *Leishmania* spp., miltefosine inhibits both phosphatidylethanolamine (PE) *N*-methyl-transferase in the PC synthetic pathway and a glycosome-located alkyl-specific acyl coenzyme A acyltransferase involved in lipid remodeling (Lux et al., 2000; Urbina, 2006) and has been reported to induce apoptosis (Verma et al., 2007).

In the model yeast *Saccharomyces cerevisiae*, deletion of the drug-specific transporter Lem3p, a functional homolog of the leishmanial LdMT-LdRos3, conferred resistance to miltefosine and reduced uptake of fluorescently labeled derivatives of PC and PE, suggesting that alkyl phospholipid analogs, including miltefosine, are internalized via Lem3p (Hanson et al., 2003). We showed previously that miltefosine inhibits phospholipase B1, a key virulence determinant of the pathogenic yeast-like fungus, *Cryptococcus neoformans*, but only at relatively high concentrations, suggesting that this is not its primary mode of action (Widmer et al., 2006b). The fungal cell targets of miltefosine are still unknown.

In this study, we demonstrate in *S. cerevisiae* that miltefosine is taken up rapidly and penetrates the mitochondrial inner membrane, where it disrupts membrane potential and causes dose-dependent inhibition of cytochrome *c* oxidase (COX) and apoptosis-like cell death. We also present evidence that the inhibition of COX by miltefosine occurs specifically at the site of subunit VIIa in the enzyme complex, which is encoded by a nuclear gene *COX9*.

Materials and Methods

Strains, Media, and Manipulations. Yeast strains used in the work are listed in Table 1. For yeast culture, complete medium contained 1% Bacto yeast extract (BD Biosciences, San Jose, CA) and 2% Bacto peptone (BD Biosciences) with 2% glucose (YPD) or glycerol (YPGly). For determination of growth on solid media, 2% Bacto agar was added. Minimal medium (YNB) contained 2% glucose and 0.67% Difco yeast nitrogen base (BD Biosciences) without amino acids. Nutrients essential for propagation of auxotrophic strains were added to YNB at 25 μg/ml for uracil and adenine and 50 μg/ml for leucine. For selection of G418 (Geneticin) resistance, the antibiotic was added to YPD at a concentration of 200 μg/ml. Standard methods were used for yeast incubation, transformation, and DNA extraction (Burke et al., 2000).

Commercial MAX Efficiency DH5α Competent Cells (Invitrogen, Mount Waverley, VIC, Australia) were used as host for plasmid propagation in *Escherichia coli*. Luria broth (Sigma-Aldrich, Sydney, NSW, Australia) was used for bacterial culture, and ampicillin was added to the culture at a final concentration of 100 μg/ml to retain plasmids containing ampicillin resistance marker. A QIAprep Spin Miniprep Kit (QIAGEN, Doncaster, VIC, Australia) was used to extract plasmid DNA from *E. coli*. Standard methods were used for DNA restriction enzyme digestion, ligation, and electrophoresis (Sambrook and Russell, 2001).

Measurement of Miltefosine Uptake. To measure miltefosine incorporation, strain M2915-6A was cultured at 30°C to a final cell density of 10^8 cells/ml (late log or early stationary phase) in a total of 50 ml of YNB broth supplemented with leucine, adenine, and uracil. ^{14}C-labeled miltefosine (42 mCi/mmol; GE Healthcare, Chalfont St. Giles, Buckinghamshire, UK) was mixed with nonlabeled miltefosine (Cayman Chemical, Ann Arbor, MI) and the mixture was added to the yeast culture to give a final miltefosine concentration of 1 μg/ml with a ^{14}C activity of 0.11 μCi/ml. At 5-min intervals, 1 ml of culture was removed and the cells were pelleted by centrifugation. The supernatant, containing unincorporated ^{14}C-miltefosine, was collected and retained. The cells were immediately washed with 1 ml of phosphate-buffered saline (PBS; Invitrogen) containing 10 mg/ml bovine serum albumin to remove nonspecifically bound drug from the surface, and the final cell pellet was dissolved in 500 μl of NCS tissue solubilizer (GE Healthcare). The buffer used to wash the cells was combined with previously retained supernatant for measuring unincorporated ^{14}C-miltefosine. The solubilized cells and the combined supernatants were each mixed with 6 ml of Ultima Gold scintillant (PerkinElmer Life and Analytical Sciences, Waltham, MA) and analyzed in a Packard Tri-Carb liquid scintillation analyzer (model 2100TR; PerkinElmer Life and Analytical Sciences) to obtain a measurement of cell-incorporated and unincorporated [^{14}C]miltefosine, respectively. Miltefosine uptake was expressed as the percentage of radioactivity incorporated by cells at each time point.

Assay of Cell Sensitivity to Miltefosine. Strain M2915-6A was cultured in YPD broth at 30°C to log phase. Cells were then harvested and resuspended in fresh YPD or YPGly at a density of 10^5 cells/ml. The cell suspensions were distributed into a 96-well plate at 50 μl/well. YPD or YPGly containing series concentrations of miltefosine was added and mixed with the cell suspensions to make the final volume 100 μl in each well and the drug concentrations from 0 to 256 μg/ml. The plate was then incubated in a moisturized container at 30°C for 4 days with vigorous shaking until the live cells reached the final stage of growth. Miltefosine sensitivity was assessed as the minimum drug concentration at which the cells were unable to grow.

Fluorescence Microscopy. Yeast cells were incubated in YPD broth with or without miltefosine at 2 μg/ml for 1 h and then stained with DAPI (Invitrogen) to visualize mitochondrial nucleoids and nuclei. $DiOC_6$ (Invitrogen) and propidium iodide (PI; Invitrogen) were also added to detect mitochondrial membrane potential and permeability of the cell membrane, according to previous publica-

TABLE 1
Yeast strains used in this work
The source for these data is the current study, unless otherwise specified.

Name	Description
M2915-6A[a]	*MATa*, *leu2*, *ade2*, *ura3*
6A-MI50-401	*MATa*, *leu2*, *ade2*, *ura3*, miltefosine-resistant
6A-[pCXJ15]	M2915-6A transformed with pCXJ15
6A-[pCXJ15-COX7]	M2915-6A transformed with pCXJ15-COX7
6A-[pCXJ15-COX8]	M2915-6A transformed with pCXJ15-COX8
6A-[pCXJ15-COX9]	M2915-6A transformed with pCXJ15-COX9
6A-[pRS416-COX9]	M2915-6A transformed with pRS416-COX9
BY4741/Δcox9[b]	*MATa*, *his3*, *leu2*, *met15*, *ura3*, *cox9*Δ::*KanMX4*
6A/Δcox9	M2915-6A with *cox9*Δ::*KanMX4*
Δcox9-[pRS416-COX9]	6A/Δcox9 transformed with pRS416-COX9
Δcox9-[pCXJ15-COX9]	6A/Δcox9 transformed with pCXJ15-COX9

[a] Chen et al., 1993.
[b] Open Biosystems.

tions (Pringle et al., 1989; Barcellona et al., 1990). In brief, yeast cells were harvested from the cultures, washed with water, and incubated for 20 min with DAPI, $DiOC_6$, and PI at concentrations of 2 μg/ml, 0.64 ng/ml, and 10 μg/ml, respectively. To immobilize cells, an equal volume of 1% low melting temperature agarose (Roche, Castle Hill, NSW, Australia), preheated at 35°C, was mixed with the stained cells before the application of the samples to the glass slides. Fluorescence was visualized under a DeltaVision RT deconvolution microscope system (Applied Precision, Inc., Issaquah, WA) fitted with a 100× oil/1.40 objective lens (Olympus, Tokyo, Japan). For DAPI, $DiOC_6$, and PI, the excitation/emission filters were set at 360/457, 490/528, and 555/617 nm, respectively. Images were acquired using Resolve3D softWoRx (version 3.7.1; Applied Precision) and Image J (version 1.43; http://rsb.info.nih.gov/ij/) at 1000× magnification and assembled with Photoshop (version 10.0; Adobe Systems, San Jose, CA) and Illustrator (version 13.0; Adobe Systems).

Assessment of Apoptosis. Apoptosis was assessed using the Vybrant FAM Caspase Assay Kit (Invitrogen) and the In Situ Cell Death Detection Kit [terminal deoxynucleotidyl transferase dUTP nick-end labeling (TUNEL) assay; Roche]. Yeast cells were cultured in YPD broth to late log phase. Two aliquots of 2.4×10^8 cells were collected by centrifugation, washed with water, and resuspended in 240 ml of YPD broth with and without 2 μg/ml miltefosine. This concentration of miltefosine was inhibitory, but not lethal, to yeast cells because growth curves remained flat over a 4-h coincubation period (data not shown). Apoptosis was measured in cultures that were incubated at 30°C with shaking. For the TUNEL assay, cells were fixed with 4% paraformaldehyde in PBS for 60 min, and the cell walls were removed by digestion with 10 mg/ml Zymolyase-20T (MP Biomedicals, Seven Hills, NSW, Australia) for 2 h at 37°C with mild shaking. The resulting spheroplasts were then treated with TUNEL reagents according to the manufacturer's instructions. For the caspase assay, live cells were labeled directly with the caspase assay reagents and 10 μg/ml PI according to the instruction manual. Flow cytometry was conducted by measuring 1.5×10^4 fluorescently labeled cells on an LSRII flow cytometer (BD Biosciences). Labeled cells were also examined by fluorescence microscopy.

Genomic Library Construction and Screening. A genomic library from strain 6A-MI50-401 was constructed using a previously published method with modifications (Jauert et al., 2005). Genomic DNA was extracted and subjected to treatment with the restriction enzyme EcoRI. To preserve genes potentially containing EcoRI sites, the genomic DNA was partially digested. Fragments ranging in size from 100 base pairs to 10 kb were purified using a QIAquick polymerase chain reaction (PCR) purification kit (QIAGEN) and ligated into EcoRI-digested pCXJ15. The ligation mixture was used to transform MAX Efficiency DH5α Competent Cells. Plasmid DNA was extracted from ampicillin-resistant colonies that had grown on Luria broth/ampicillin agar plates for 15 h at 37°C, and the DNA concentration was adjusted to 200 μg/ml. The plasmid DNA from 10 individual transformations was then pooled to form the final genomic library. The quality of the library was validated by comparing the electrophoresis profile of the EcoRI-released library inserts with that of the EcoRI-digested genomic DNA.

To screen for genes in which overexpression confers miltefosine resistance in yeast, strain M2915-6A was transformed with the resulting genomic library. Ura^+ transformants were first grown on YNB agar plates without uracil at 30°C until the average colony size reached approximately 2 mm in diameter. The colonies were then replica plated onto YNB plates containing 20 μg/ml miltefosine and incubated at 30°C for 2 days. Ura^+ colonies that also grew in the presence of miltefosine were selected, and their resistance phenotype was confirmed by performing a serial dilution drop test (Zuo et al., 2007) on YNB containing miltefosine. Total DNA containing the plasmids from the miltefosine resistant isolates was purified and used to transform the MAX Efficiency DH5α Competent Cells. Plasmid DNA was then retrieved from the resulting ampicillin resistant colonies. The genomic inserts conferring the miltefosine resistance phenotype were then determined by DNA sequencing and BLAST search in the *S. cerevisiae* Genome Database (http://www.yeastgenome.org/).

Cloning of COX7 and COX8. PCR fragments containing *COX7* or *COX8* were amplified using primer pairs ScCOX7 FP1 and RP1 or ScCOX8 FP1 and RP1 (Table 2), respectively. An EcoRI site was designed at the 5′ end of each primer. PCRs were conducted using a T-Gradient PCR machine (Biometra GmbH, Goettingen, Germany) with standard protocol. Products of *COX7* and *COX8* genes, both with a size of 1.2 kb, were treated with EcoRI and ligated into the corresponding site of pCXJ15 to generate pCXJ15-COX7 and pCXJ15-COX8, respectively.

Quantitative Real-Time PCR. Total RNA was prepared from yeast transformants 6A-[pCXJ15-COX7], 6A-[pCXJ15-COX8], 6A-

TABLE 2
PCR primers used in this work
Underlined nucleotides in the primers are the sequences matching the yeast genome.

Name	Use	Nucleotide Sequence (5′–3′)
ScCOX7	Cloning of *COX7*	
FP1		CCCGGGGAATTCGGAGGAGTAATCTTTTCAGT
RP1		CCCGGGGAATTCCACAAGAATCAACAGCAACA
ScCOX8	Cloning of *COX8*	
FP1		CCCGGGGAATTCAATGCAAGCATCAAGAGCAA
RP1		CCCGGGGAATTCACTCATTGCAACAAAGTAAACTGC
Sc cox9	Disruption of *COX9*	
FP1		GGATTGTAAGACACCTTTAT
RP1		CTGTCTTATTCTCCACATACA
Sc cox9	Confirmation of Δ*cox9*	
FP2		ATACTCATGCTGGGCGATCT
RP2		GATGGGAATATACCTGCGAA
ScACT1	qRT-PCR for *ACT1*	
QRP1		ACGTGAGTAACACCATCACCGGAA
QFP1		ACGTTCCAGCCTTCTACGTTTCCA
ScCOX7	qRT-PCR for *COX7*	
QRP1		TAGAAGTGGTGTAACGACGGCTAC
QFP1		CTATGGTGGAGACATCCAAGGTCA
ScCOX8	qRT-PCR for *COX8*	
QRP1		GCAAATCCAATAGCGAAGAACCCG
QFP1		GAGGTCAGTACACTTCAAAGACGGTG
ScCOX9	qRT-PCR for *COX9*	
QRP1		GCTAGCTCTGCGTAGAACTTCTCT
QFP1		AGAGTCATCATGGACATCGTCCTC

[pCXJ15-COX9], and 6A-[pCXJ15] using TRIzol reagent (Invitrogen) according to the manufacturer's instructions. RNA concentration and purity were determined using a NanoPhotometer (Implen GmbH, Munich, Germany), and an A_{260}/A_{280} ratio of 1.9 or greater was indicative of a sufficient purity for quantitative real-time PCR (qRT-PCR). An amount of 5 μg of total RNA from each strain was treated with DNase I (amplification grade; Invitrogen) and used as a template for oligo-dT-primed cDNA synthesis using the SuperScript III First-Strand Synthesis System (Invitrogen). RNase H (Invitrogen) was then used to remove the RNA component in the RNA/cDNA complex. Standard curves were prepared using equal amounts of cDNA from all strains to obtain final concentrations of 100, 20, 4, 0.8, and 0.16 ng/μl. For individual samples, cDNA from each strain was diluted to a final concentration of 4 ng/μl. A volume of 5 μl of each standard and sample was then used as a template for qRT-PCR using Platinum SYBR Green qPCR SuperMix-UDG (Invitrogen). The primers used are listed in Table 2. The PCR conditions were adjusted in accordance with the instructions from the manufacturers. Thermo cycling was set at 95°C for 15 s and 60°C for 45 s, and a total of 40 cycles was conducted on a Rotor-Gene 6000 RT-PCR machine (Corbett Research, Sydney, NSW, Australia). Data were then obtained and analyzed using the Rotor-Gene 6000 Series software (version 1.7; Corbett Research). For all tested transformants, *COX* gene expressions were normalized to the expression of the house-keeping gene *ACT1* using the standard curves and calculated by taking the expressions in 6A-[pCXJ15] as basal levels.

COX9 Deletion. To generate a Δ*cox9*-null mutant in the background of M2915-6A, a PCR-based method using a *KanMX4* cassette (Wach et al., 1994) was used to disrupt *COX9* in the strain. A 2.1-kb fragment containing *KanMX4* disrupted *COX9* (*cox9*Δ::*KanMX4*) was amplified from the commercially available strain, BY4741/Δcox9 (Open Biosystems, Huntsville, AL). The primers used were Sc cox9 FP1 and RP1 (Table 2). The PCR product was then transformed into M2915-6A to replace the endogenous 0.7-kb *COX9* region by homologous recombination. Δ*cox9* mutants were selected on the basis of stable G418 resistance. To confirm disruption of *COX9*, PCR primer pair Sc cox9 FP2 and RP2 (Table 2), annealing to the 5′ and 3′ flanking sequences of the disrupted locus, respectively, was used to visualize a 2.5-kb DNA fragment in place of a 1.1-kb fragment in the WT.

Preparation of Mitochondria and Postmitochondrial Membranes. Mitochondrial fractions were prepared from 500-ml cultures grown to late log phase in YPD broth at 30°C (Clark-Walker et al., 2000). In brief, cells were harvested, resuspended in 30 ml of suspension buffer [1.2 M sorbitol, 20 mM *N*-tris-[hydroxymethyl] methyl-2-aminoethanesulfonic acid (TES), and 14 mM β-mercaptoethanol, pH 7.4] containing 10 mg/ml Zymolyase-20T and incubated at 35°C for 60 min to allow cell wall digestion. The resulting spheroplasts were resuspended in 30 ml of ice-cold homogenization buffer [0.6 M sorbitol, 10 mM TES, 0.1 mM 4-[2-aminoethyl]-benzenesulfonylfluoride·HCl (AEBSF), pH 7.4] and ruptured in a Dounce homogenizer with 30 strokes. Mitochondria were pelleted by centrifugation at 9000*g* for 20 min after prior removal of cellular debris by two 5-min rounds of centrifugation at 3500 and 5000*g*, respectively. Mitochondria were resuspended in 200 μl of mitochondrion buffer (5 mM TES, 150 mg/ml glycerol, 0.5 mM EDTA, 0.5 mM dithiothreitol, and 0.1 mM AEBSF, pH 7.5) and stored at −80°C. The postmitochondrial supernatant was then centrifuged at 100,000*g* to obtain membrane enriched pellet.

COX Assay. A commercial cytochrome *c* oxidase assay kit (Sigma-Aldrich) was used to measure the enzyme activity in mitochondrial fractions and examine the inhibition of the enzyme by KCN (Sigma-Aldrich) and miltefosine. For the COX activity assay, standard procedures provided by the manufacturer were followed. For COX inhibition, mitochondrial fractions were solubilized with 1 mM *n*-dodecyl-β-D-maltoside, and total protein content was measured using the Better Bradford Assay Kit (Thermo Fisher Scientific, Waltham, MA). The protein concentration of each mitochondrial preparation was adjusted to 4 μg/ml using 1× enzyme dilution buffer supplied with the kit, and a volume of 20 μl, equivalent to 80 ng of protein, was added to each reaction in a 96-well plate. KCN and miltefosine were diluted in 1× assay buffer and then mixed with reduced cytochrome *c* to give the series concentrations of KCN from 0 to 10 mM and miltefosine from 0 to 256 μg/ml, respectively, and a final reduced cytochrome *c* concentration of 20 μM. The total volume of each reaction was 220 μl and COX activity was monitored at 5-min intervals over a 4-h period at room temperature by measuring the absorbance at a wavelength of 550 nm (A_{550}) using a plate reader (VMax with SOFTmax PRO, version 4.8; Molecular Devices, Sunnyvale, CA) to determine the amount of reduced cytochrome *c* remaining in the reaction. The COX activity was calculated according to the definition of Sigma-Aldrich.

Results

Miltefosine-Induced Mitochondrial Disruption and Apoptosis-Like Cell Death. We first determined the kinetics of cellular uptake of ^{14}C-labeled miltefosine by *S. cerevisiae*. Under the conditions specified, more than 60% of a saturating concentration of [^{14}C]miltefosine was taken up within 5 min, reaching a plateau within 10 to 20 min (Fig. 1A). To demonstrate that membrane-associated miltefosine was preferentially localized in mitochondria, we removed extracellular ^{14}C-miltefosine after 30 min incubation by backwashing the cells with PBS containing 10 mg/ml bovine serum albumin, disrupted the cell walls, and prepared mitochondrial and membrane fractions by differential centrifuga-

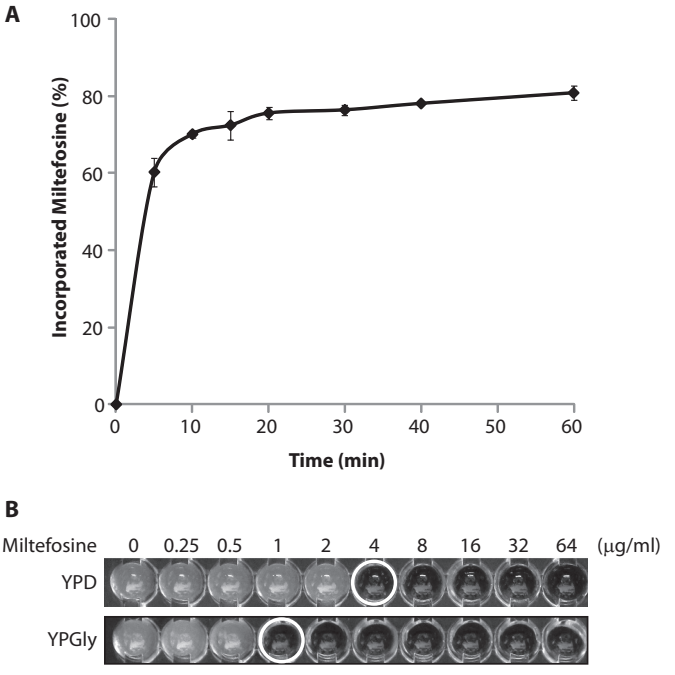

Fig. 1. Miltefosine incorporation into yeast and drug sensitivity of the cells. A, yeast cells cultured to late log phase in YNB broth were incubated with 1 μg/ml ^{14}C-labeled miltefosine at 30°C for the times indicated. At each time point, the cell-associated [^{14}C]miltefosine was measured by scintillation counting. Error bars represent S.D. (n = 3). Note that more than 60% of the drug was incorporated into the cells within 5 min. B, in a 96-well plate, in each well, 100 μl of YPD or YPGly broth containing miltefosine at the concentrations indicated was inoculated with 5 × 10^3 yeast cells. The plate was then incubated at 30°C with vigorous shaking until the growth of the cells had reached the final stage (4 days). Note that turbidity within a well is indicative of cell growth that is not inhibited by the drug. White circles indicate the wells containing the minimum concentrations of miltefosine required to inhibit cell growth.

tion, as described under *Materials and Methods*. Approximately 10% of the internalized drug was present in the mitochondrial fraction and 5% in the membrane fraction, confirming an enrichment in mitochondria (data not shown). To examine whether internalized miltefosine differentially targets metabolic pathways specific for fermentation or respiration, drug sensitivity of *S. cerevisiae* growing on different carbon sources was assessed. Yeast cells were reproducibly four times more sensitive to miltefosine in YPGly medium in which the carbon source was nonfermentable glycerol, compared with cells growing in YPD where the carbon source was fermentable glucose. In YPGly, cells were inhibited by $\geq$1 μg/ml miltefosine, whereas in YPD, cells were suppressed by $\geq$4 μg/ml the drug (Fig. 1B).

The effect of miltefosine on the function of mitochondria is shown in Fig. 2. Healthy mitochondrial nucleoids in untreated cells were visualized microscopically by DAPI staining, as a bright punctate network of small spots. A tubular structure connecting the nucleoids was observed with $DiOC_6$, indicative of functional mitochondria with strong membrane potential. As expected, PI, a membrane-impermeant fluorescent dye, was not taken up by the untreated cells, indicative of cell viability.

After treatment with miltefosine for 1 h, three different cell populations were distinguishable by their staining patterns (Table 3). In the majority of the cells (approximately 68%), a diffuse DAPI and $DiOC_6$ staining pattern was observed, indicative of mitochondrial damage and disruption of mitochondrial membrane potential. However, this cell population was PI-negative, indicating that the cell membranes were physically intact. Only in a small population of the cells (approximately 13%) were the punctate structures of the mitochondria, as visualized with DAPI and $DiOC_6$, still visible, although with reduced numbers of nucleoids, indicative of miltefosine-affected, but functional, mitochondria. Approximately 19% of the miltefosine-treated cells were PI-positive, indicative of disrupted plasma membrane integrity and presumably cell death. These cells were stained nonspecifically with DAPI and $DiOC_6$ (Fig. 2).

To confirm that miltefosine induces apoptosis-like cell death in yeast, two intrinsic markers of apoptosis, caspase activation and nuclear DNA fragmentation, were sought in miltefosine-treated and untreated cells using flow cytometry and fluorescence microscopy (Fig. 3). Microscopic examination of spheroplasts subjected to TUNEL revealed a subpopulation of cells with increased fluorescence after miltefosine treatment, indicative of TUNEL-specific DNA fragmentation. Activation of caspase was observed in miltefosine-treated whole cells. These results were confirmed by flow cytometry (Fig. 3).

Identifying COX9 as a Potential Target of Miltefosine. To identify molecular targets of miltefosine, a genomic library housed within a high copy number shuttle vector, pCXJ15 (Chen, 1996), was constructed from a yeast strain, 6A-MI50-401. The library was then used to transform a wild-type (WT) miltefosine-sensitive strain, M2915-6A, to screen for clones conferring miltefosine resistance. Transformants were identified by their ability to grow in the presence of 20 μg/ml miltefosine, a concentration of the drug 10 times greater than the MIC (Widmer et al., 2006a). Individual plasmids were isolated from miltefosine-resistant transformants, and the DNA sequences of the inserts were determined. One of the plasmids contained a 1.8-kb DNA insert, and a BLAST search against the *Saccharomyces cerevisiae* Genome Database revealed that it contained the gene *COX9* (locus tag YDL067C; SGDID: S000002225) encoding the critical VIIa subunit (Cox9p) of the COX complex in the mitochondrial electron transport chain. This plasmid was later designated pCXJ15-COX9. DNA sequence analysis also confirmed that no mutation was inadvertently introduced into the *COX9* fragment during the construction of the library, and that *COX9*'s own native promoter and terminator regulated its expression from the plasmid.

To confirm that only the overexpression of *COX9* subunit in the COX complex confers resistance to miltefosine, two closely related genes, *COX7* and *COX8*, coding for adjacent subunits within the COX complex were PCR-amplified and cloned into pCXJ15, creating pCXJ15-COX7 and pCXJ15-COX8, respectively. Strain M2915-6A was transformed with PCXJ15-COX7, pCXJ15-COX8, and pCXJ15-COX9 individually. Overexpression of *COX7*, *COX8*, and *COX9* in the Ura^+ transformants was confirmed by qRT-PCR. Results showed that the transcription levels of *COX7*, *COX8*, and *COX9* were 9-, 3.7-, and 6.7-fold higher in the transformants carrying pCXJ15-COX7, pCXJ15-COX8, and pCXJ15-COX9, respectively, compared with the native levels in the control pCXJ15 transformants. 6A-[pCXJ15], 6A-[pCXJ15-COX7], 6A-[pCXJ15-COX8], and 6A-[pCXJ15-COX9] were examined on YNB plates, with or without 20 μg/ml miltefosine, using a serial dilution drop test (Zuo et al., 2007). The miltefosine-resistant phenotype of yeast transformants containing pCXJ15-COX9 was confirmed and is shown in Fig. 4. No miltefosine resistance was observed with transformants containing pCXJ15-COX7 or pCXJ15-COX8.

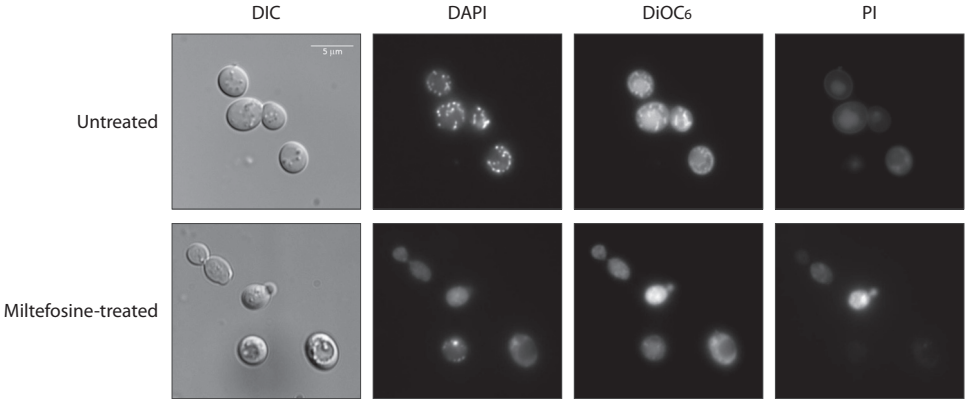

Fig. 2. Disruption of mitochondrial function by miltefosine. Yeast cells were incubated with 2 μg/ml miltefosine in YPD broth for 1 h and stained with DAPI (to visualize mitochondrial and nuclear DNA), $DiOC_6$ (to visualize mitochondrial membrane potential), and PI (to detect cell viability via cell membrane permeability). Controls (Untreated) contained no miltefosine. Fluorescence microscope images show that miltefosine treatment disrupted mitochondrial membrane potential (lower panel of $DiOC_6$ staining), diffused mitochondrial nucleoids (lower panel of DAPI staining), and increased membrane permeability (lower panel of PI staining).

COX9 Gene Dosage and Cellular Respiration. To investigate the role of Cox9p in cellular respiration, a Δ*cox9* deletion mutant was generated from strain M2915-6A. Successful gene disruption was confirmed by PCR (Supplemental Fig. 1). The resulting mutant, 6A/Δcox9, was tested for growth phenotype and respiratory competence on rich medium containing nonfermentable glycerol as the carbon source. The Δ*cox9* mutant failed to grow on YPGly despite prolonged incubation, indicating a failure of respiration (Fig. 5). To determine whether the respiratory deficiency could be restored, the *COX9* gene was subcloned from the high copy number plasmid, pCXJ15-COX9, into a low copy number shuttle vector, pRS416 (Sikorski and Hieter, 1989), and both pRS416-COX9 and pCXJ15-COX9 were introduced into 6A/Δcox9. Ura$^+$ transformants of Δcox9-[pRS416-COX9] and Δcox9-[pCXJ15-COX9] were then subcultured on YPGly for assessment of growth phenotype and respiratory competence. The low copy number plasmid, pRS416-COX9, complemented the respiratory deficiency of 6A/Δcox9, the transformants exhibiting a growth rate similar to that of the parent strain, M2915-6A, and forming normal colonies on YPGly. It is noteworthy that the growth rate of Δcox9-[pCXJ15-COX9] on YPGly was slower than Δcox9-[pRS416-COX9] (Fig. 5).

To confirm that overexpression of *COX9* compromises growth and to investigate a possible gene dosage effect, the WT strain M2915-6A was transformed with pRS416-COX9 and pCXJ15-COX9, and Ura$^+$ transformants of 6A-[pRS416-COX9] and 6A-[pCXJ15-COX9] were both assessed for growth on YPGly. Although untransformed M2915-6A, containing only one copy of the native *COX9*, showed normal growth, colonies of the transformant 6A-[pRS416-COX9] containing both native *COX9* and a low copy number of pRS416-COX9 were slightly smaller than those of M2915-6A. 6A-[pCXJ15-COX9], containing multiple copies of *COX9*, exhibited a growth defect qualitatively similar to that of Δcox9-[pCXJ15-COX9].

TABLE 3

Microscopic assessment of mitochondrial disruption by miltefosine

Average cell numbers with S.D. (n = 3) are presented. Functional mitochondria are shown in Fig. 2 as networks of punctate bright spots (DAPI) connected by tubular structures ($DiOC_6$). Disrupted mitochondria have a diffuse staining pattern in Fig. 2 with both DAPI and $DiOC_6$ staining. PI$^+$ cells are presumed dead.

	Untreated	Miltefosine-Treated
		%
PI$^-$ cells with healthy mitochondria	≥98.0	12.8 ± 1.0
PI$^-$ cells with disrupted mitochondria	≤2.0	68.2 ± 1.8
PI$^+$ cells	≤0.3	19.0 ± 2.4

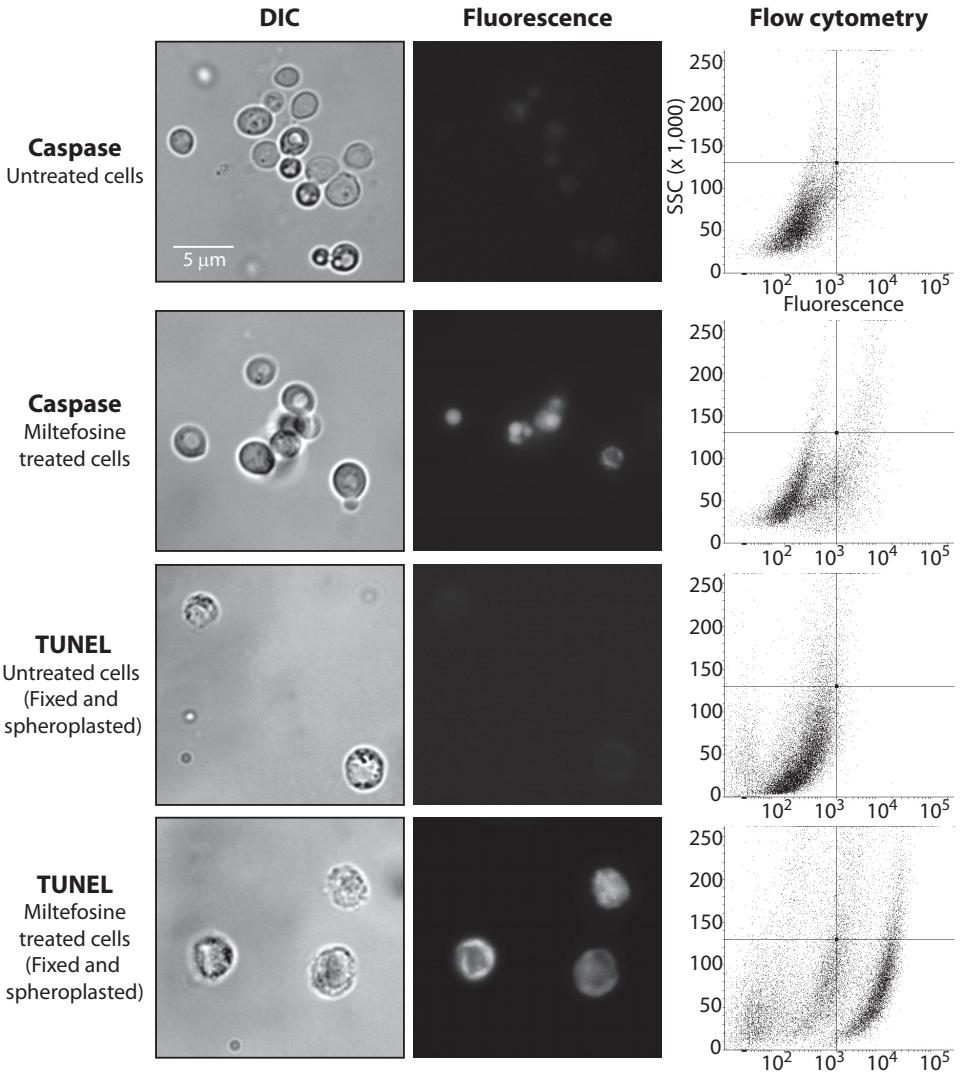

Fig. 3. Apoptosis caused by miltefosine. Cells were treated with 2 μg/ml miltefosine or no drug at 30°C for 4 h and examined for TUNEL or caspase activation by fluorescence microscopy and flow cytometry. For the TUNEL assay, cells were fixed with paraformaldehyde and spheroplasted before labeling. Representative views of the microscopy are shown. Dot plots of fluorescence intensity versus side scatter (SSC) obtained with flow cytometry demonstrate that, in miltefosine-treated samples, 12% of the cells were caspase-activated and 40% of the cells were TUNEL-positive.

Cox9p-Dependent Inhibition of COX by Miltefosine. To examine whether miltefosine treatment affects COX activity, mitochondria were isolated from the WT strain M2915-6A and subjected to a mild detergent treatment to release the COX complex from membrane lipid bilayers (Musatov et al., 2000). COX activity in the mitochondrial suspension was determined spectrophotometrically, using a cytochrome *c* oxidase assay kit (Sigma-Aldrich), to be approximately 0.25 units/mg protein (Sigma-Aldrich definition). The mitochondrial suspension was then incubated with miltefosine at concentrations ranging from 0 to 256 μg/ml or with the COX inhibitor KCN at concentrations ranging from 0 to 10 mM. The COX activity time courses clearly demonstrate that the enzyme in the WT strain was inhibited by both KCN and miltefosine in a dose-dependent manner (Fig. 6, A-1 and B-1, respectively). Although a high concentration of KCN (10 mM) caused a complete inhibition of the COX activity, a high dose of miltefosine (256 μg/ml) suppressed the enzyme by approximately 60%, reaching a level similar to the COX activity in the Δ*cox9* mutant (Fig. 6B-2).

To determine whether inhibition of COX by miltefosine is dependent on the presence of Cox9p, mitochondria prepared from 6A/Δcox9 were examined for COX activity in the presence of the drug. When *COX9* was deleted from the genome, the activity of the COX was reduced to below 40% (Fig. 6B-2). Without Cox9p, the residual COX activity was inadequate to sustain aerobic cellular respiration, because 6A/Δcox9 was unable to grow on YPGly at 30°C (Fig. 5). It is noteworthy that in the absence of Cox9p, the residual COX activity was not inhibited by miltefosine (Fig. 6B-2) but was suppressed by KCN (Fig. 6A-2).

To investigate the effect of *COX9* expression level on miltefosine-COX interaction, mitochondria from Δcox9-[pRS416-COX9] were extracted and assayed for COX activity in the presence of miltefosine. Under conditions mimicking the endogenous expression level of Cox9p using the low copy number plasmid, the miltefosine-COX dose response was restored to WT level (Fig. 6B-4), consistent with the restoration of the growth phenotype observed on YPGly (Fig. 5) and indicative of a fully functional COX. The miltefosine-COX dose response observed in mitochondria derived from 6A-[pRS416-COX9], which carried low copies of *COX9* on the plasmid, did not differ significantly from that of the WT strain (Fig. 6B-3).

The COX activity of the mitochondria extracted from Δcox9-[pCXJ15-COX9], where Cox9p was overexpressed as a result of multiple plasmid copies, was restored to approximately 70% of WT (Fig. 6B-6). However, mitochondria de-

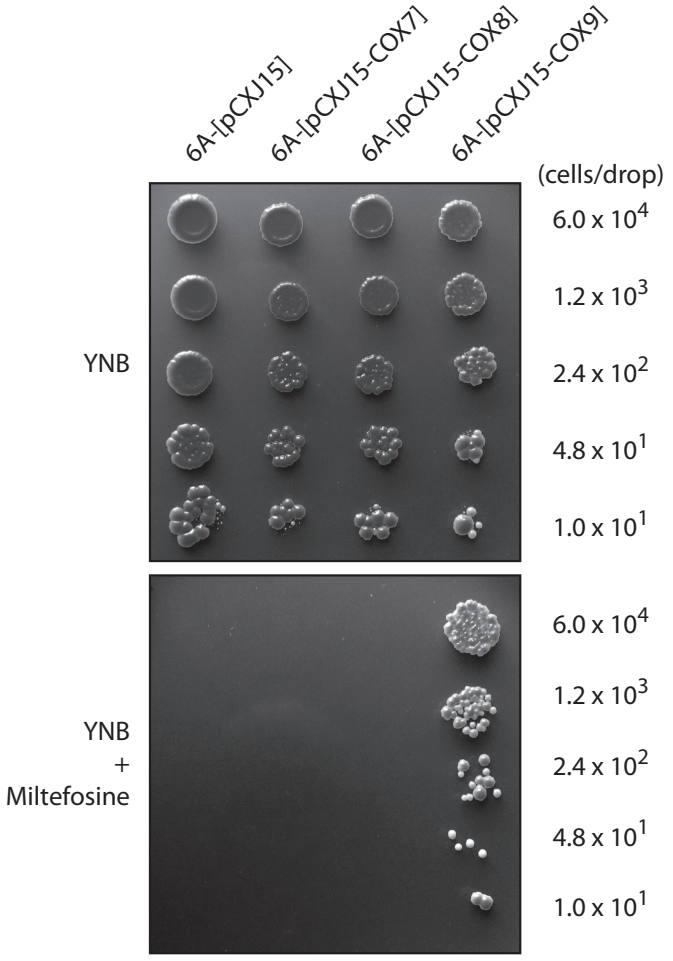

Fig. 4. Miltefosine resistance conferred by *COX9* overexpression. YNB plates containing 20 μg/ml miltefosine or no drug with drops of serially diluted M2915-6A transformants of pCXJ15-COX7, pCXJ15-COX8, and pCXJ15-COX9 are shown. 6A-[pCXJ15] was used for comparison. Photos were taken with a PowerShot A720 IS digital camera (Canon, Tokyo, Japan) after incubation at 30°C for 3 days. Note that only 6A-[pCXJ15-COX9] showed miltefosine resistance.

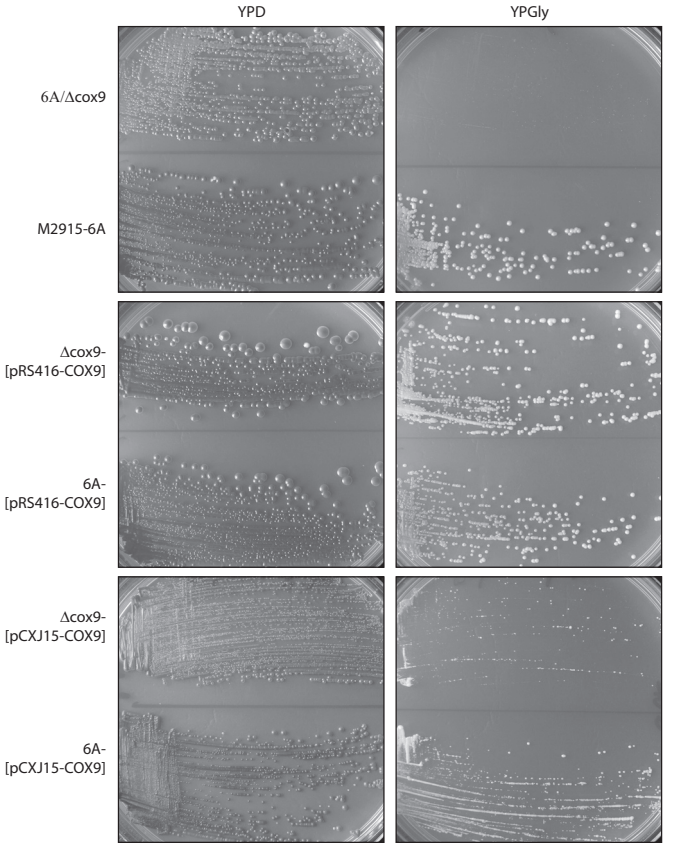

Fig. 5. *COX9* gene dosage on cellular respiration. Growth of the Δ*cox9* mutant and its parental strain on YPD (left) and YPGly (right) are shown. The effect of gene dosage is present in strains transformed with either a low copy number plasmid pRS416-COX9 or a high copy number plasmid pCXJ15-COX9 (as indicated in the square brackets). After 5-day incubation at 30°C, photos were taken using a digital camera. Note that a functional *COX9* on a low copy number plasmid restored respiration in the Δ*cox9* mutant. Respiration was reduced in transformants containing more than one copy of *COX9*.

rived from 6A-[pCXJ15-COX9], which also contained overexpressed Cox9p, displayed COX activity similar to that of WT mitochondria (Fig. 6B-5). Dose response of the enzyme to miltefosine from both transformants was evident.

Discussion

Miltefosine is a potential lead compound for new antifungal drug development (Obando et al., 2007). It has clinically useful activity against another lower eukaryote, *Leishmania* spp., but undesirable toxicities (Sindermann and Engel, 2006). Understanding its mode of action is essential to the design of analogs with increased antifungal potency and reduced toxicity. Our data indicate that miltefosine induces apoptosis-like cell death in the model yeast, *S. cerevisiae,* as a result of a specific interaction with the Cox9p subunit of mitochondrial COX.

Miltefosine Penetrates Mitochondria and Disrupts Mitochondrial Function. Internalization of miltefosine by fungi has not previously been studied directly, although it has been shown in *S. cerevisiae* that fluorescently labeled analogs of PC are transported across the plasma membrane to the cytosolic leaflet by a protein-mediated, energy-dependent mechanism and that these analogs are distributed subsequently to the nuclear envelope/ER and mitochondria (Grant et al., 2001). The protein Lem3p was later identified as a specific membrane transporter for PC, PE, and, presumably, miltefosine, because deletion of *LEM3* conferred resistance to miltefosine (Hanson et al., 2003). *LEM3* is a member of an evolutionarily conserved gene family and has two homologs in *S. cerevisiae*.

In the present study, uptake of [^{14}C]miltefosine by yeast cells was very rapid and reached plateau within 10 to 20 min. This is consistent with internalization of miltefosine via a saturable, active transport channel, presumably involving Lem3p. Because mitochondria are widely distributed double-membrane networks within cells and form a large part of the cellular membrane system, it is probable that, after internalization, miltefosine distributes along the lipid bilayers of the mitochondria and interacts with potential drug targets, both

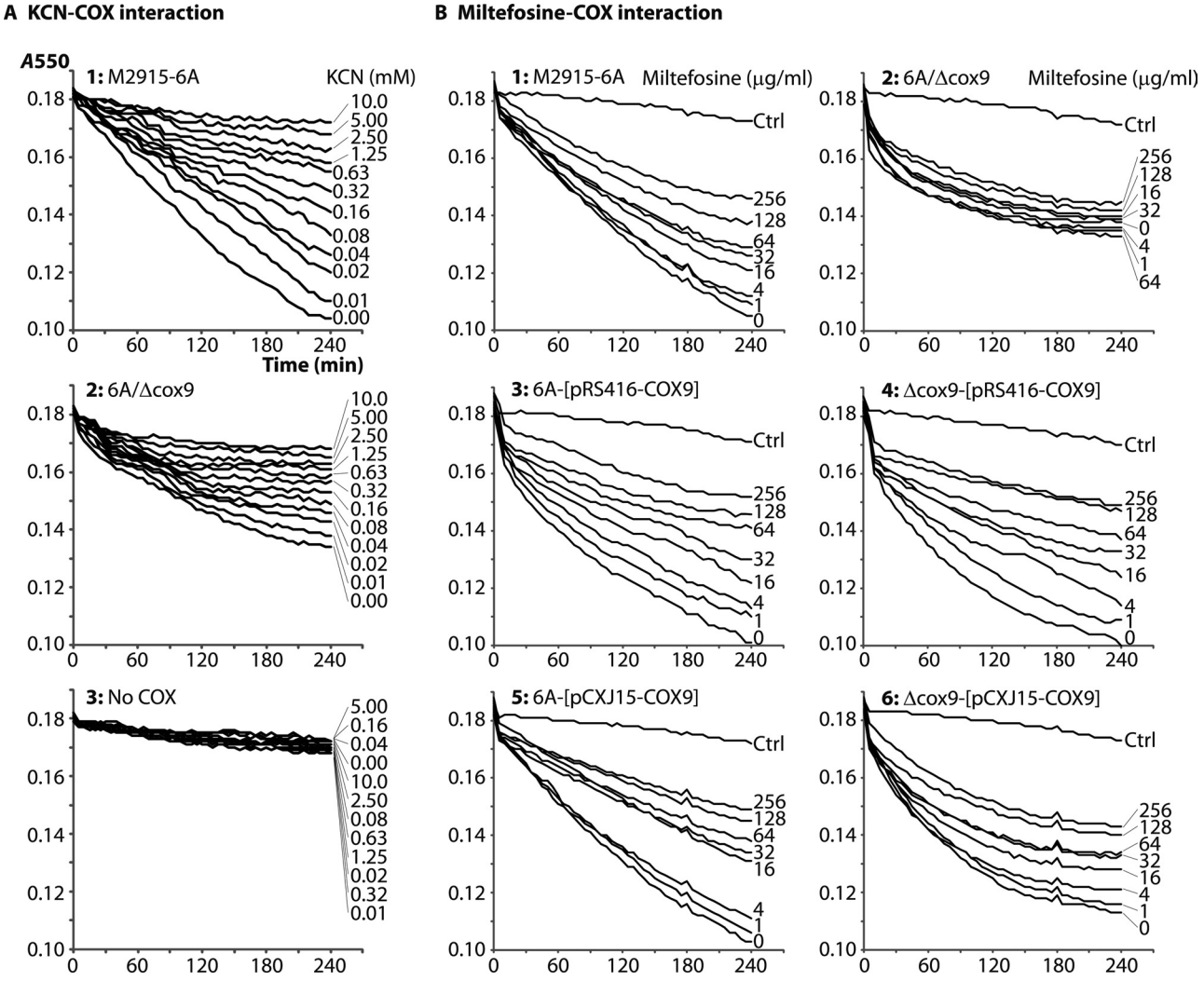

Fig. 6. Cox9p-dependent miltefosine-COX dose response. Mitochondrial fractions were extracted from the strains indicated and dissolved in enzyme dilution buffer with 1 mM *n*-dodecyl-β-D-maltoside. COX activity in the mitochondria was measured using a cytochrome *c* oxidase assay kit. A, time-course plots of COX inhibition by KCN at various concentrations are shown, taking samples with no COX as controls. Note that in the absence of Cox9p, the remaining COX activity in 6A/Δcox9 was still sensitive to KCN. B, time-course plots of COX activity at different concentrations of miltefosine are shown. Controls without COX are labeled as Ctrl. Note that miltefosine inhibited COX in a dose-dependent manner only when Cox9p was present.

on the membranes and in the matrix. Our data indeed showed that more than 10% of internalized [^{14}C]miltefosine localized to subcellular mitochondrial fraction of the cell lysates.

An effect of miltefosine on mitochondrial function was clearly demonstrated, because yeast cells growing by respiration, relying heavily on mitochondrial function, were four times more sensitive to miltefosine than cells growing by fermentation (Fig. 1B). A selective effect of miltefosine on mitochondria was demonstrated by staining cells with DAPI and $DiOC_6$, which revealed that miltefosine penetrated into the mitochondrial inner membrane, causing disruption of the membrane potential and dispersal of mitochondrial nucleoids within the matrix (Fig. 2).

Miltefosine Causes Apoptosis-Like Cell Death in Yeast. There is little doubt that miltefosine causes apoptosis in both cancer cells and leishmanial parasites (Barratt et al., 2009). However, the biochemical basis of apoptosis in these cells, in particular whether it occurs as a direct consequence of inhibition of PC synthesis, remains controversial (van der Sanden et al., 2004).

Apoptosis has been reported in a range of yeast including *S. cerevisiae*, *Schizosaccharomyces pombe*, and *Candida albicans* (Ramsdale, 2008). *S. cerevisiae* has been used as the model system since the characterization of the *CDC48* mutation that led to the discovery of apoptosis in yeasts (Madeo et al., 2004). Genes involved in programmed cell death in *S. cerevisiae* have also been identified as apoptotic regulators in mammalian cells, indicating that the basic apoptotic machinery is indeed present and functional.

In the present study, a miltefosine concentration of 2 μg/ml clearly caused apoptosis-like cell death, as demonstrated by disruption of mitochondrial function and miltefosine-induced nuclear damage (Fig. 2). TUNEL-specific fragmentation of DNA and activation of cellular caspases were obvious in miltefosine-treated cell cultures (Fig. 3). These observations are typical signs of apoptosis in yeast (Thevissen et al., 2008). Furthermore, miltefosine directly inhibited COX located on the mitochondrial inner membrane (Fig. 6). Our results suggest that, as a result of direct interaction between the drug and COX, miltefosine disrupts mitochondrial homeostasis and triggers apoptotic signaling.

Cox9p Is the Inhibition Site of COX by Miltefosine. The COX enzyme complex catalyzes the final step of respiration, transferring electrons from cytochrome *c* to molecular oxygen. By coupling electron transfer to proton translocation from the mitochondrial matrix to the intermembrane space, COX maintains the electrochemical potential required by the oxidative phosphorylation system for the synthesis of ATP. Because most human invasive fungal pathogens grow only by cellular respiration, fungus-specific components of the COX complex would be potentially novel antifungal drug targets. Our data demonstrate that the inhibition of COX activity by miltefosine is dose-dependent and relies on the presence of Cox9p (Fig. 6). As possible Cox9p homologs in other eukaryotes have substantially diverged from those in fungi, Cox9p is potentially a fungus-specific subunit of the COX complex targetable by the drugs.

Because COX is a polymeric enzyme, with subunits encoded by either the nucleus or the mitochondria, its assembly is complex, highly regulated, and requires coordination between both organelles (Fontanesi et al., 2006). Crystallization of bovine COX has provided detailed insight into its three-dimensional organization (Tsukihara et al., 1996). In *S. cerevisiae*, 11 subunits of the enzyme complex have been identified. Three large subunits, Cox1p, Cox2p, and Cox3p, which form the catalytic core, are encoded by the mitochondrial genome and synthesized within the matrix. It has been reported that the catalytic core is embedded within the inner membrane. The heme and copper cofactors, which are involved in the electron transport activity of the COX complex, are coordinated by Cox1p and Cox2p. Other small subunits, including Cox7p, Cox8p, and Cox9p, are nuclear-encoded, synthesized in the cytoplasm, and imported into the mitochondria. These small subunits are associated with the hydrophobic core and are essential for the assembly and stability of the holoenzyme. The small subunits are also involved in the modulation of catalytic activity and protection of the core from damaging reactive oxygen species.

In this study, *COX9* was isolated from a genetic screen for possible molecular targets of miltefosine. *COX9* has previously been cloned and is present as a single copy in the haploid genome of *S. cerevisiae* (Wright et al., 1986). Our results demonstrate that Cox9p is essential for maintaining a fully functional COX assembly and that the level of Cox9p expression affects yeast cellular respiration (Fig. 5). In the Δ*cox9* mutant, the growth arrest correlated with a >60% loss of COX activity, indicating that this level of COX inhibition was sufficient to prevent oxidative phosphorylation. This level of inhibition was also detected in WT COX treated with high concentrations of miltefosine. In the absence of Cox9p, the remaining COX activity was not further inhibited by miltefosine but was sensitive to KCN, implicating Cox9p as the site within COX responsible for the miltefosine dose-dependent inhibition (Fig. 6).

Restoration of Cox9p expression in the Δ*cox9* mutant by an exogenous *COX9* in low copy number completely restored COX functionality and cellular respiration. The miltefosine-COX dose response of the transformants was also similar to that of WT COX. Overexpression of Cox9p in 6A-[pCXJ15-COX9] and Δcox9-[pCXJ15-COX9] resulted in defective growth on nonfermentable carbon source, suggesting that the *COX9* copy number is crucial for optimal cellular respiration and hence growth and that overexpression of the gene is detrimental. COX activity in the *COX9* overexpression strain 6A-[pCXJ15-COX9] was similar to that of the WT strain, but in Δcox9-[pCXJ15-COX9], it was 70% of WT. Although this result might indicate a biased preference by the COX for chromosomally expressed Cox9p, when Cox9p was overexpressed, there was a clear miltefosine-COX dose response. Taken together, these results indicate that regulation of the cellular level of Cox9p is critical for optimal COX function, and that changes in Cox9p levels are likely to render the COX complex unstable.

It has been proposed that mature Cox9p is a 6.3-kDa amphiphilic peptide of 54 amino acids, with an internal hydrophobic domain and hydrophilic N and C termini. This structural motif is similar to that of Cox7p and Cox8p. Cox9p, together with Cox7p and Cox8p, form a transmembrane intermediate subassembly that spans the lipid bilayer of the inner membrane (Power et al., 1986) and is therefore accessible to miltefosine. Our results showed that overexpression of only Cox9p, but not Cox7p and Cox8p, confers miltefosine resistance in yeast cells. It seems likely that miltefosine-

Cox9p binding reduces the amount of Cox9p available for assembly of functional enzyme complexes; hence, COX becomes structurally unstable and vulnerable to proteolysis. Plasmid-derived Cox9p can compensate for the loss of native Cox9p bound to miltefosine, because transformants containing pCXJ15-COX9 were resistant to miltefosine, whereas cells with pCXJ15-COX7 or pCXJ15-COX8 were still sensitive to the drug (Fig. 4).

In summary, we conclude that Cox9p is a target of the antifungal drug miltefosine. We propose that interaction between Cox9p and miltefosine disrupts the electron transport chain by causing partial disassembly of COX, ultimately leading to an apoptosis-like cell death.

Acknowledgments

We thank J. Munro, M. Karam, N. Pantarat, C. Biswas, C. F. Wilson, Y. Koda, F. Widmer, and H. Yu for technical assistance and advice. We also thank S. Lev for proofreading the manuscript.

Authorship Contributions

Participated in research design: Zuo, Djordjevic, Jolliffe, and Sorrell.

Conducted experiments: Zuo, Bijosono Oei, Desmarini, and Schibeci.

Performed data analysis: Zuo, Djordjevic, Schibeci, and Sorrell.

Wrote or contributed to the writing of the manuscript: Zuo, Djordjevic, Jolliffe, and Sorrell.

Other: Djordjevic, Jolliffe, and Sorrell acquired funding for the research.

References

Barcellona ML, Cardiel G, and Gratton E (1990) Time-resolved fluorescence of DAPI in solution and bound to polydeoxynucleotides. *Biochem Biophys Res Commun* **170:**270–280.

Barratt G, Saint-Pierre-Chazalet M, and Loiseau PM (2009) Cellular transport and lipid interactions of miltefosine. *Curr Drug Metab* **10:**247–255.

Burke D, Dawson D and Stearns T (2000) *Methods in Yeast Genetics*: *A Cold Spring Harbor Laboratory Course Manual.* Cold Spring Harbor Laboratory Press, Cold Spring Harbor, NY.

Chen SC and Sorrell TC (2007) Antifungal agents. *Med J Aust* **187:**404–409.

Chen XJ (1996) Low- and high-copy-number shuttle vectors for replication in the budding yeast *Kluyveromyces lactis. Gene* **172:**131–136.

Chen XJ, Guan MX, and Clark-Walker GD (1993) *MGM101*, a nuclear gene involved in maintenance of the mitochondrial genome in *Saccharomyces cerevisiae. Nucleic Acids Res* **21:**3473–3477.

Clark-Walker GD, Hansbro PM, Gibson F, and Chen XJ (2000) Mutant residues suppressing ρ^0-lethality in *Kluyveromyces lactis* occur at contact sites between subunits of F_1-ATPase. *Biochim Biophys Acta* **1478:**125–137.

Croft SL, Seifert K, and Duchêne M (2003) Antiprotozoal activities of phospholipid analogues. *Mol Biochem Parasitol* **126:**165–172.

de Castroa SL, Santa-Ritaa RM, Urbinab JA, and Croftc SL (2004) Antiprotozoal lysophospholipid analogues: a comparison of their activity against trypanosomatid parasites and tumor cells. *Mini Rev Med Chem* **4:**141–151.

Fontanesi F, Soto IC, Horn D, and Barrientos A (2006) Assembly of mitochondrial cytochrome c-oxidase, a complicated and highly regulated cellular process. *Am J Physiol Cell Physiol* **291:**C1129–C1147.

Grant AM, Hanson PK, Malone L, and Nichols JW (2001) NBD-labeled phosphatidylcholine and phosphatidylethanolamine are internalized by transbilayer transport across the yeast plasma membrane. *Traffic* **2:**37–50.

Hanson PK, Malone L, Birchmore JL, and Nichols JW (2003) Lem3p is essential for the uptake and potency of alkylphosphocholine drugs, edelfosine and miltefosine. *J Biol Chem* **278:**36041–36050.

Jauert PA, Jensen LE, and Kirkpatrick DT (2005) A novel yeast genomic DNA library on a geneticin-resistance vector. *Yeast* **22:**653–657.

Kesson AM, Bellemore MC, O'Mara TJ, Ellis DH, and Sorrell TC (2009) Scedosporium prolificans osteomyelitis in an immunocompetent child treated with a novel agent, hexadecylphospocholine (miltefosine), in combination with terbinafine and voriconazole: a case report. *Clin Infect Dis* **48:**1257–1261.

Lux H, Heise N, Klenner T, Hart D, and Opperdoes FR (2000) Ether-lipid (alkylphospholipid) metabolism and the mechanism of action of ether–lipid analogues in *Leishmania. Mol Biochem Parasitol* **111:**1–14.

Madeo F, Herker E, Wissing S, Jungwirth H, Eisenberg T, and Fröhlich KU (2004) Apoptosis in yeast. *Curr Opin Microbiol* **7:**655–660.

Musatov A, Ortega-Lopez J, and Robinson NC (2000) Detergent-solubilized bovine cytochrome c oxidase: dimerization depends on the amphiphilic environment. *Biochemistry* **39:**12996–13004.

Obando D, Widmer F, Wright LC, Sorrell TC, and Jolliffe KA (2007) Synthesis, antifungal and antimicrobial activity of alkylphospholipids. *Bioorg Med Chem* **15:**5158–5165.

Pérez-Victoria FJ, Gamarro F, Ouellette M, and Castanys S (2003) Functional cloning of the miltefosine transporter. A novel P-type phospholipid translocase from *Leishmania* involved in drug resistance. *J Biol Chem* **278:**49965–49971.

Power SD, Lochrie MA, and Poyton RO (1986) The nuclear-coded subunits of yeast cytochrome *c* oxidase. The amino acid sequences of subunits VII and VIIa, structural similarities between the three smallest polypeptides of the holoenzyme, and implications for biogenesis. *J Biol Chem* **261:**9206–9209.

Pringle JR, Preston RA, Adams AE, Stearns T, Drubin DG, Haarer BK, and Jones EW (1989) Fluorescence microscopy methods for yeast. *Methods Cell Biol* **31:**357–435.

Ramsdale M (2008) Programmed cell death in pathogenic fungi. *Biochim Biophys Acta* **1783:**1369–1380.

Ruiter GA, Zerp SF, Bartelink H, van Blitterswijk WJ, and Verheij M (1999) Alkyl-lysophospholipids activate the SAPK/JNK pathway and enhance radiation-induced apoptosis. *Cancer Res* **59:**2457–2463.

Sambrook J and Russell DW (2001) *Molecular Cloning*: *A Laboratory Manual.* Cold Spring Harbor Laboratory Press, Cold Spring Harbor, NY.

Sikorski RS and Hieter P (1989) A system of shuttle vectors and yeast host strains designed for efficient manipulation of DNA in *Saccharomyces cerevisiae. Genetics* **122:**19–27.

Sindermann H and Engel J (2006) Development of miltefosine as an oral treatment for leishmaniasis. *Trans R Soc Trop Med Hyg* **100 (Suppl 1):**S17–S20.

Thevissen K, Madeo F, Ludovico P, Cammue B, and Winderickx J (2008) Joined in death: highlights of the Sixth International Meeting on Yeast Apoptosis in Leuven, Belgium, 30 April-4 May 2008. *Yeast* **25:**927–934.

Tong Z, Widmer F, Sorrell TC, Guse Z, Jolliffe KA, Halliday C, Lee OC, Kong F, Wright LC, and Chen SC (2007) In vitro activities of miltefosine and two novel antifungal biscationic salts against a panel of 77 dermatophytes. *Antimicrob Agents Chemother* **51:**2219–2222.

Tsukihara T, Aoyama H, Yamashita E, Tomizaki T, Yamaguchi H, Shinzawa-Itoh K, Nakashima R, Yaono R, and Yoshikawa S (1996) The whole structure of the 13-subunit oxidized cytochrome c oxidase at 2.8 A. *Science* **272:**1136–1144.

Unger C and Eibl H (1991) Hexadecylphosphocholine: preclinical and the first clinical results of a new antitumor drug. *Lipids* **26:**1412–1417.

Urbina JA (2006) Mechanisms of action of lysophospholipid analogues against trypanosomatid parasites. *Trans R Soc Trop Med Hyg* **100 (Suppl 1):**S9–S16.

van Blitterswijk WJ and Verheij M (2008) Anticancer alkylphospholipids: mechanisms of action, cellular sensitivity and resistance, and clinical prospects. *Curr Pharm Des* **14:**2061–2074.

van der Sanden MH, Houweling M, Duijsings D, Vaandrager AB, and van Golde LM (2004) Inhibition of phosphatidylcholine synthesis is not the primary pathway in hexadecylphosphocholine-induced apoptosis. *Biochim Biophys Acta* **1636:**99–107.

Verma NK, Singh G, and Dey CS (2007) Miltefosine induces apoptosis in arsenite-resistant *Leishmania donovani* promastigotes through mitochondrial dysfunction. *Exp Parasitol* **116:**1–13.

Wach A, Brachat A, Pöhlmann R, and Philippsen P (1994) New heterologous modules for classical or PCR-based gene disruptions in *Saccharomyces cerevisiae. Yeast* **10:**1793–1808.

Widmer F, Hartmann M, Frey B, and Kölliker R (2006a) A novel strategy to extract specific phylogenetic sequence information from community T-RFLP. *J Microbiol Methods* **66:**512–520.

Widmer F, Wright LC, Obando D, Handke R, Ganendren R, Ellis DH, and Sorrell TC (2006b) Hexadecylphosphocholine (miltefosine) has broad-spectrum fungicidal activity and is efficacious in a mouse model of cryptococcosis. *Antimicrob Agents Chemother* **50:**414–421.

Wieder T, Reutter W, Orfanos CE, and Geilen CC (1999) Mechanisms of action of phospholipid analogs as anticancer compounds. *Prog Lipid Res* **38:**249–259.

Wright RM, Dircks LK, and Poyton RO (1986) Characterization of *COX9*, the nuclear gene encoding the yeast mitochondrial protein cytochrome c oxidase subunit VIIa. Subunit VIIa lacks a leader peptide and is an essential component of the holoenzyme. *J Biol Chem* **261:**17183–17191.

Zuo X, Xue D, Li N, and Clark-Walker GD (2007) A functional core of the mitochondrial genome maintenance protein Mgm101p in *Saccharomyces cerevisiae* determined with a temperature-conditional allele. *FEMS Yeast Res* **7:**131–140.

Address correspondence to: Tania C. Sorrell, Centre for Infectious Diseases and Microbiology, Westmead Millennium Institute and Sydney Emerging Infections and Biosecurity Institute, University of Sydney, NSW 2145, Australia. E-mail: tania.sorrell@sydney.edu.au